Promotion of Homologous Recombination by SWS-1 in Complex with RAD-51 Paralogs in *Caenorhabditis elegans*

T. Brooke McClendon,*,†,1 Meghan R. Sullivan,*,‡,1 Kara A. Bernstein,*,‡,2 and Judith L. Yanowitz*,†,2

*Molecular Genetics and Developmental Biology Graduate Program, †Magee-Womens Research Institute and Department of Obstetrics, Gynecology, and Reproductive Sciences, and ‡University of Pittsburgh Cancer Institute and Department of Microbiology and Molecular Genetics, University of Pittsburgh School of Medicine, Pittsburgh, Pennsylvania 15213

ORCID IDs: 0000-0002-8865-0731 (T.B.M.); 0000-0002-0814-6755 (M.R.S.); 0000-0001-6886-8787 (J.L.Y.)

ABSTRACT Homologous recombination (HR) repairs cytotoxic DNA double-strand breaks (DSBs) with high fidelity. Deficiencies in HR result in genome instability. A key early step in HR is the search for and invasion of a homologous DNA template by a single-stranded RAD-51 nucleoprotein filament. The Shu complex, composed of a SWIM domain-containing protein and its interacting RAD51 paralogs, promotes HR by regulating RAD51 filament dynamics. Despite Shu complex orthologs throughout eukaryotes, our understanding of its function has been most extensively characterized in budding yeast. Evolutionary analysis of the SWIM domain identified *Caenorhabditis elegans sws-1* as a putative homolog of the yeast Shu complex member Shu2. Using a CRISPR-induced nonsense allele of *sws-1*, we show that *sws-1* promotes HR in mitotic and meiotic nuclei. *sws-1* mutants exhibit sensitivity to DSB-inducing agents and fail to form mitotic RAD-51 foci following treatment with camptothecin. Phenotypic similarities between *sws-1* and the two RAD-51 paralogs *rfs-1* and *rip-1* suggest that they function together. Indeed, we detect direct interaction between SWS-1 and RIP-1 by yeast two-hybrid assay that is mediated by the SWIM domain in SWS-1 and the Walker B motif in RIP-1. Furthermore, RIP-1 bridges an interaction between SWS-1 and RFS-1, suggesting that RIP-1 facilitates complex formation with SWS-1 and RFS-1. We propose that SWS-1, RIP-1, and RFS-1 compose a *C. elegans* Shu complex. Our work provides a new model for studying Shu complex disruption in the context of a multicellular organism that has important implications as to why mutations in the human RAD51 paralogs are associated with genome instability.

KEYWORDS homologous recombination; RAD51 paralog; Shu complex; camptothecin; helq-1

DNA double-strand breaks (DSBs) are extremely cytotoxic lesions that threaten genome integrity. DSBs arise from both endogenous sources, such as replicative damage, or exogenous sources, such as ionizing radiation (IR) and chemotherapeutic agents. To ensure the maintenance of the genome, DSBs need to be repaired by high-fidelity repair pathways, the most robust of which is homologous recombination (HR), in which DNA from a sister chromatid or homologous chromosome provides a repair template. Initial processing of DSB ends by resection forms 3′ single-stranded DNA (ssDNA) overhangs that are coated with the ssDNA-binding protein RPA. The exchange of RPA for the recombinase enzyme RAD51 facilitates the homology search and strand invasion of homologous DNA templates to form displacement loop structures. Subsequent stabilization of HR intermediates then requires removal of RAD51 from the double-stranded DNA to allow access to the DNA polymerization machinery. Given the central role of the RAD51 filament in HR, its assembly and disassembly are tightly regulated to ensure the fidelity of repair (Krejci *et al.* 2012; Jasin and Rothstein 2013; Heyer 2015).

Key mediators of RAD51 filament assembly are the RAD51 paralogs. In humans, there are six RAD51 paralogs: RAD51B, RAD51C, RAD51D, XRCC2, XRCC3, and the newly identified

doi: 10.1534/genetics.115.185827
Manuscript received December 7, 2015; accepted for publication February 19, 2016; published Early Online March 1, 2016.
Supplemental material is available online at www.genetics.org/lookup/suppl/doi:10.1534/genetics.115.185827/-/DC1.
[1]These authors contributed equally to this work.
[2]Corresponding authors: Magee-Womens Research Institute, Department of Obstetrics, Gynecology, and Reproductive Sciences, University of Pittsburgh School of Medicine, 204 Craft Ave., Pittsburgh, PA 15213. E-mail: jly@alum.mit.edu; Department of Microbiology and Molecular Genetics, University of Pittsburgh School of Medicine, 5117 Centre Ave., Pittsburgh, PA 15213. E-mail: karab@pitt.edu

SWSAP1 (Liu *et al.* 2011; Karpenshif and Bernstein 2012; Prakash *et al.* 2015). The RAD51 paralogs form multiple subcomplexes including a novel complex containing SWSAP1 and its binding partner SWS1 (Miller *et al.* 2002; Liu *et al.* 2011). Mutations in the RAD51 paralogs are associated with cancer predisposition and, in some cases, Fanconi anemia-like syndromes (Vaz *et al.* 2010; Wang *et al.* 2015), underscoring the importance of these proteins in maintaining genome stability. Nevertheless, progress in understanding the roles of these complexes in metazoans has been hampered by the embryonic lethality observed in mouse knockouts and the difficulty in attaining purified proteins for biochemical studies (Deans *et al.* 2000; Thacker 2005; Kuznetsov *et al.* 2009; Suwaki *et al.* 2011).

Much of our understanding of the RAD51 paralogs comes from studies in budding yeast in which the Rad51 paralogs form two subcomplexes, the Shu complex (also called the PCSS complex) and the Rad55–Rad57 complex. The Shu complex is an obligate hetero-tetramer composed of Psy3, Csm2, Shu1, and Shu2, which facilitates HR-mediated DSB repair by stimulating Rad51 filament formation (Shor *et al.* 2005; Mankouri *et al.* 2007; Ball *et al.* 2009; Godin *et al.* 2013, 2015; Hong and Kim 2013; Sasanuma *et al.* 2013; Gaines *et al.* 2015). Csm2 and Psy3 are Rad51 paralogs whereas Shu2 is a member of the SWS1 protein family, defined by a highly conserved SWIM domain (Makarova *et al.* 2002; Martin *et al.* 2006; Godin *et al.* 2015). Yeast with Shu complex disruptions exhibit sensitivity to the alkylating agent methylmethane sulfonate (MMS), increased mutations, decreased meiotic crossover (CO) formation, and reduced spore viability (Shor *et al.* 2005; Hong and Kim 2013; Sasanuma *et al.* 2013; Godin *et al.* 2015). Unlike yeast and humans, only two RAD-51 paralogs, RFS-1 and RIP-1, are known in *Caenorhabditis elegans*. Both paralogs function in HR, mediating repair of DNA lesions in the mitotic and meiotic regions of the worm germline (Ward *et al.* 2007, 2010; Yanowitz 2008; Taylor *et al.* 2015). Nevertheless, the relationship of the RAD-51 paralogs to a worm Shu complex remains largely unknown.

Although Shu complex function was thought to be conserved throughout eukaryotes, the poor amino acid conservation across species precluded identification of functional paralogs in other systems until recently. Evolutionary analyses of the SWIM domain led to the identification of *C. elegans sws-1* as the homolog of *Saccharomyces cerevisiae* Shu2 (Godin *et al.* 2015). *C. elegans* provides several advantages for probing the function of *sws-1*. The germline is spatially and temporally organized such that the stages of meiotic prophase I—and their integrity—can be readily distinguished by DNA morphology (visualized by DAPI). The germline is a reliable source of programmed DSBs induced by the topoisomerase-like SPO-11 (Keeney *et al.* 1997), and HR is the favored repair mechanism due to the need to form crossovers between homologous chromosomes (Cole *et al.* 2010). Populations of *C. elegans* exist primarily as self-fertilizing hermaphrodites with two X chromosomes; rare nondisjunction of the X chromosome (<0.2% in wild type) results in viable males with a single X chromosome (XO). Nondisjunction of autosomes, by contrast, is lethal in most cases and can be ascertained by the presence of unhatched eggs (Hodgkin *et al.* 1979). Thus, progeny viability and male frequency [*h*igh *i*ncidence of *m*ales (Him) phenotype] can intimate meiotic HR repair defects, although those phenotypes are not sufficient indicators on their own.

Using CRISPR/Cas9, we created a nonsense allele of *sws-1* in *C. elegans* and probed the role of this conserved DNA repair factor in both mitotic and meiotic cells of the germline. We find that *sws-1* is the functional homolog of *S. cerevisiae* Shu2, showing that (1) *sws-1* mutants exhibit DNA damage sensitivity; (2) disruption of *sws-1* results in reduced RAD-51 foci formation following camptothecin (CPT) treatment; and (3) SWS-1 interacts with the known *C. elegans* RAD-51 paralogs RFS-1 and RIP-1 (Ward *et al.* 2007; Taylor *et al.* 2015). Our findings show for the first time the mitotic and meiotic role of *sws-1* in the context of a metazoan and expand upon the known RAD-51 paralog-interacting proteins in worms.

Materials and Methods

Culture and strains

For all experiments, worms were cultured on NGM plates seeded with OP50 and grown at 20° unless otherwise noted (Brenner 1974). Mutant strains used in this study were the following: LG I, *syp-3(ok758)*, *dog-1(gk10)*; LG III, *rip-1(tm2948)*, *rfs-1(ok1372)*, *helq-1(tm2134)*; LG V, *sws-1(ea12)* (generation of strain described below); and LG X, *unc-58(e665)*. *rip-1*, *rfs-1 rip-1*, and *helq-1* were kindly provided by Simon Boulton; *syp-3* by Sarit Smolikove; and *dog-1* by Ann Rose. Other strains were provided by the *Caenorhabditis* Genetics Center. Double and triple mutants generated for this work were done so using standard genetic techniques and are listed in Supplemental Material, Table S1. *helq-1;sws-1* double mutants were maintained as heterozygotes due to lack of suitable genetic balancers and were genotyped in all experiments to confirm homozygosity of markers. Control animals used in this study are the homozygous wild-type self-progeny of an *sws-1* heterozygote and did not differ phenotypically from our N2 stock (Table 1, rows A and B).

Generation of sws-1(ea12)

Unique CRISPR guides near the start and stop codons of *sws-1* were selected using the CRISPR design tool at http://crispr.mit.edu (see Table S2 for sequences of the primers used in single guide RNA design) . Primers were inserted into pDD162 (P*eft-3*::*Cas9*::*tbb-2* 3′ UTR) using the Q5 Site-Directed Mutagenesis Kit (NEB) as described (Dickinson *et al.* 2013). DNA from positive clones was isolated using the PureLinkHQ Mini Plasmid DNA Purification Kit (Invitrogen) and sequenced to verify the insertion. An injection mix consisting of 30 ng/μl *dpy-10(cn64)* repair oligo (Arribere *et al.* 2014) and 50 ng/μl each genomic RNA (gRNA) in pDD162 (one for *dpy-10*, two for *sws-1*) diluted in PureLink EB buffer (Invitrogen) was prepared

Table 1 General characteristics of strains used in this study

Row	Genotype	*n*	Average brood ± SEM	% lethal ± SEM (normalized)	% male ± SEM
A	N2	12	232.42 ± 5.97	0.00 ± 0.67	0.07 ± 0.05
B	Wild type	6	227.17 ± 9.28	0.56 ± 1.49	0.16 ± 0.16
C	*sws-1*	25	203.84 ± 10.35	8.45 ± 2.05*	0.63 ± 0.08*
D	*rip-1*	6	265.33 ± 8.02	6.33 ± 1.11	1.78 ± 0.72
E	*rip-1;sws-1*	16	268.00 ± 9.72	2.59 ± 0.49	0.87 ± 0.10
F	*rfs-1*	10	212.90 ± 7.59	9.36 ± 1.48	2.22 ± 0.31
G	*rfs-1;sws-1*	13	206.77 ± 9.59	7.84 ± 2.00	1.78 ± 0.26
H	*rfs-1,rip-1*	11	177.00 ± 9.00	8.47 ± 1.29	2.20 ± 0.31
I	*rfs-1,rip-1;sws-1*	22	164.23 ± 9.97	12.33 ± 1.94	2.43 ± 0.29

Brood size, lethality, and male frequency were collected as described in *Materials and Methods* (*n* = number of worms). "% lethal ± SEM" is normalized to N2 (row A) to account for a 3% counting error. Differences between wild type and *sws-1* were assessed by Mann–Whitney (*$P < 0.05$); differences in lethality and male frequency among genetic combinations of *sws-1*, *rip-1*, and *rfs-1* were assessed using one-way ANOVA with multiple comparisons (Table S3 and Table S4).

and injected into N2 day 1 adult hermaphrodites. Roller progeny [*dpy-10(cn64)/+*] of injected hermaphrodites were isolated and allowed to lay eggs before being lysed in buffer for DNA isolation (0.1 M Tris, pH 8.5, 0.1 M NaCl, 0.05 M EDTA, 1% SDS, 0.1 μg/ml proteinase K). A region ~300 bp around each Cas9 target site was amplified by PCR and resolved on a 2–3% agarose gel to identify products differing in size from an uninjected control (Table S2 and Figure 1, A and B). This approach yielded one candidate founder strain with an insertion near the start codon; we did not detect any mutations near the stop codon (data not shown). PCR product from the founder strain was purified (NucleoSpin Gel and PCR Clean-up Kit, Macherey-Nagel), sequenced, and aligned with wild-type sequence to identify mutations. The candidate allele was outcrossed to N2 multiple times to lose the *dpy-10(cn64)* allele and any potential (although unanticipated) off-target mutations (Paix *et al.* 2014).

Gene expression

A population of ~1000 day 1 adult hermaphrodites were washed three times in 1× M9 buffer (3 g/liter KH2PO4, 6 g/liter Na2HPO4, 5 g/liter NaCl, 1 mM MgSO4), resuspended in Trizol (Invitrogen), and vortexed for ~60 sec before being flash-frozen and stored at −80°. Worms were further disrupted by three freeze–thaw cycles in which samples were thawed in cold water, vortexed 30 sec, and frozen at −80°. RNA was isolated by chloroform extraction and isopropanol precipitation and resuspended in nuclease-free water. Genomic DNA was removed using the DNaseI kit (Sigma-Aldrich, AMPD1-1KT) according to the manufacturer's instructions. RNA quality was measured by a spectrophotometer.

Reverse transcription was performed using the TaqMan High Capacity RNA-to-cDNA kit (Applied Biosystems) according to the manufacturer's instructions. Comparative threshold cycle (C_T) experiments were performed according to the manufacturer's instructions using TaqMan Fast Universal No AmpErase UNG PCR Master Mix and TaqMan gene expression assays for CELE_Y39B6A.40 (*sws-1*) and reference gene *rpl-32* (Hoogewijs *et al.* 2008) (Thermo Fisher Scientific). Reactions were run in triplicate and analyzed with Applied Biosystems Fast PCR System and StepOne Software using the comparative CT method (Schmittgen and Livak 2008).

Brood size/lethality/him frequency

L4 hermaphrodites of a given genotype were individually plated and transferred to a clean plate every 12 hr until egg laying ceased. After transfer, the number of eggs and L1's on the plate was counted and recorded. Three to four days later, each plate was scored for the number of adult hermaphrodites and males. Time-point data from each individual parent was combined to give total eggs, total adult brood, and total males. Percentage of hatching was calculated by dividing total adults by total eggs, multiplying by 100, and then subtracting from 100 to give the percentage of lethality. Percentage of lethality was normalized to N2 to account for 3% error in egg counts. To calculate male frequency, the total number of males was divided by the total number of adults. The data are presented as the mean ±SEM from isogenic parents.

Developmental arrest assay

Developmental arrest in unstressed larvae was assayed as previously described (Craig *et al.* 2012). Briefly, 100 L1 larvae of a given genotype were plated onto center-seeded 3-cm dishes in triplicate. After 48–60 hr, the number of adult, L3–L4, and L1–L2 worms on each plate was counted. To calculate larval arrest, the number of worms in each developmental stage was divided by the total number of worms counted.

Mutation frequency

Mutation frequency of *sws-1(ea12)* was assessed as described previously (Harris *et al.* 2006). Briefly, *sws-1(ea12);unc-58(e665)* and *unc-58(e665)* homozygotes were grown on 40 6-cm plates until starvation and then transferred by chunking to ~100 10-cm plates containing a streak of OP50 opposite the agar chunk. Plates were scored by eye for the presence of Unc revertants that could reach the OP50. Mutation frequency was calculated as described (Harris *et al.* 2006). Mutation frequency of *sws-1(ea12)* in the *dog-1* background was assessed as described previously (Youds *et al.* 2006). Briefly, generation-matched (F_3) *dog-1(gk10)* and *dog-1(gk10);sws-1(ea12)* day 1 adults were individually lysed in buffer for DNA isolation. The poly G/C tract of *vab-1* was amplified by PCR (primers and conditions

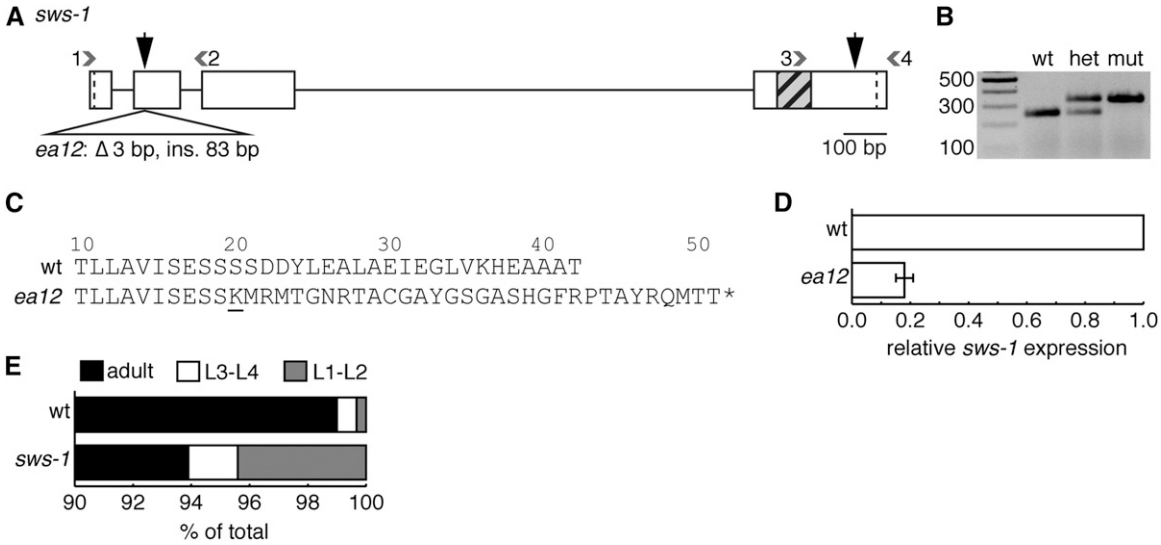

Figure 1 *sws-1(ea12)* is an insertion/deletion that results in an early stop codon. (A) Diagram of *sws-1*-coding region. Boxes and straight lines represent exons and introns, respectively. Start and stop codons are demarcated by dashed lines. Gray hatched box shows DNA encoding the SWIM domain. Large black vertical arrows mark predicted Cas9 cleavage sites for each injected gRNA; small gray numbered arrowheads represent primers used for screening (primer sequences are listed in Table S2). *ea12* is a 3-bp deletion/83-bp insertion in exon 2. (B) Representative image of *ea12* genotyping using primer combination 1 and 2 as shown in A. The mutant allele is readily detected as the slower migrating band on a 2% agarose gel. (C) Predicted protein sequence of exon 2 of wt (top) and *ea12* (bottom) SWS-1. *sws-1(ea12)* is predicted to produce the first 19 amino acids of the wild-type SWS-1 protein followed by 32 frameshifted amino acids prior to truncation (underlined letter marks beginning of frameshift). (D) Expression of *sws-1* mRNA in wild-type and *sws-1(ea12)* hermaphrodites. The data are presented as the mean expression of *sws-1* relative to reference gene *rpl-32* ± SEM for two biological replicates. (E) Developmental progression of wild type and *sws-1*. For each genotype, 100 L1's were plated in triplicate and scored 50 hr later as L1–L2, L3–L4, or adult. The results shown are the percentage of total worms in each developmental stage. A subset of *sws-1* mutants arrested as L1–L2 larvae ($P < 0.001$ *vs.* wt, Fisher's exact test).

described in Youds *et al.* 2006) and resolved on a 1.5% agarose gel. The presence of one or more bands below the expected product size signified a deletion event.

Genotoxin sensitivity assays

Details for each genotoxin exposure are described below. In all assays, the number of eggs and L1's were counted at the end of the collection window. Three to four days later, each plate was scored for the number of adult progeny. Survival was calculated as the number of adult progeny divided by the number of eggs/L1's relative to untreated worms ±SEM from 22 to 50 adults over two trials.

Ionizing radiation

L4 hermaphrodites were plated on each of four 6-cm plates with 30–100 worms/plate depending on genotype and IR dose. The following day, worms were exposed to 0, 10, 50, or 100 Gy of IR from a 137Cs source (Gammacell1000 Elite, Nordion International Inc.). Twelve hours post-irradiation, worms were plated (two worms per 3-cm dish) and allowed to lay for 12 hr before removal and egg counts.

Methyl methanesulfonate

L4 hermaphrodites were incubated in 0, 0.0025, 0.005, and 0.01% MMS (50-9480886, Fisher Healthcare) dissolved in 1× M9 buffer for 12 hr at room temperature with mild agitation. Following exposure, worms were washed, transferred to plates, and allowed to recover for 12 hr. Post recovery, worms were plated (two worms per 3-cm dish) and allowed to lay for 12 hr before removal and egg counts.

Camptothecin

CPT exposure was performed as described with minor alterations (Kessler and Yanowitz 2014). Briefly, young adult hermaphrodites were incubated in 0, 250, 500, and 1000 nM CPT (ICN15973250, Fisher Healthcare) dissolved in 1× M9, pH 6.0, buffer and 0.2% DMSO for 18 hr at room temperature with mild agitation. Following exposure, worms were washed, transferred to plates, and allowed to recover for 3 hr. Post recovery, worms were plated (five worms per 3-cm dish) and allowed to lay for 4 hr before removal and egg counts.

To assess DNA damage-induced apoptosis in response to CPT, young adult hermaphrodites were treated, washed, and allowed to recover as described above. Post recovery, worms were exposed to acridine orange (AO) (Invitrogen A3568) as previously described (Lant and Derry 2014). Worms that were verified to have taken up the stain were mounted in levamisole and observed on a compound microscope with fluorescence. Cells in the pachytene–diplotene region of the germline that retained AO were scored as apoptotic. The data are presented as mean AO-positive nuclei ± SEM from 25 germlines.

Hydroxyurea

Hydroxyurea (HU) (H8627, Sigma-Aldrich) was dissolved in ~60° NGM to final concentrations of 0, 8, 12, and 25 mM, poured into 3-cm dishes to solidify, and used within 24 hr.

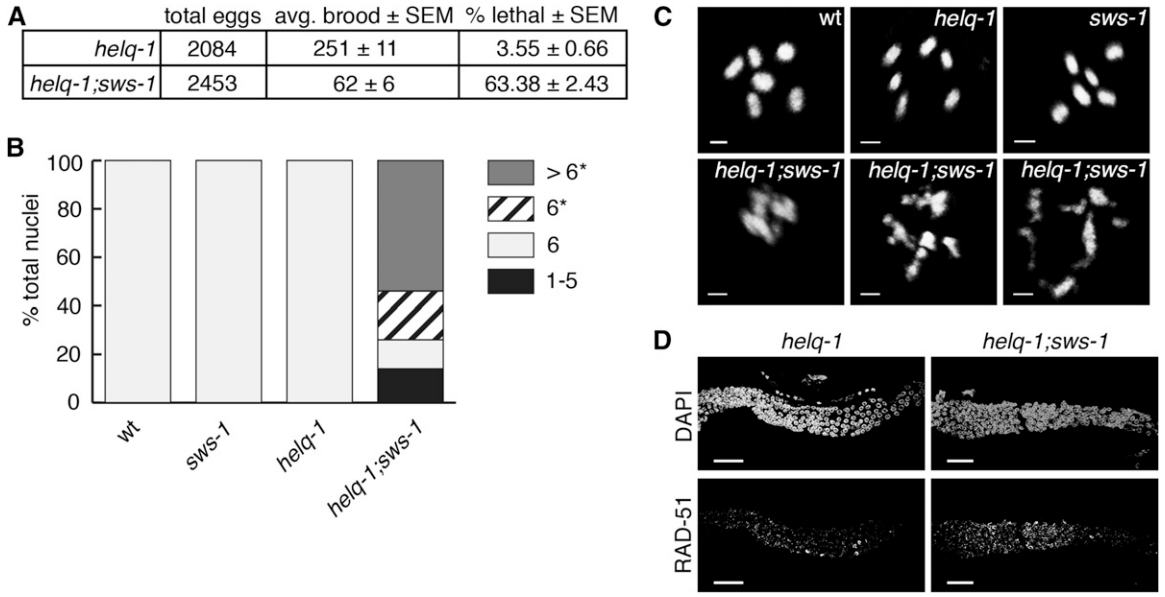

Figure 2 *sws-1* is synthetic lethal with *helq-1*. (A) Brood size and viability of *helq-1* and *helq-1;sws-1* mutants. (B) Quantification of the number of DAPI-staining bodies at diakinesis in wild-type, *sws-1*, *helq-1*, and *helq-1;sws-1* germlines. Only the −1 oocyte was used for analysis (n = 20 for wild type (wt) and *helq-1*; n = 50 for *sws-1* and *helq-1;sws-1*). Asterisk indicates chromosomal abnormalities. (C) Representative images of −1 oocytes analyzed as described in B. Bar, 2 μm. (D) Representative images of RAD-51 foci from the transition zone (left) to late pachytene (right) in *helq-1* and *helq-1;sws-1* germlines. Bar, 20 μm.

Plates were seeded with heat-killed OP50 (Kessler and Yanowitz 2014) and dried for 45–60 min under a fume hood. L4 hermaphrodites were incubated on HU plates for 20 hr at 20°. Following exposure, worms were moved to plates with drug-free NGM and live OP50 (two to four worms per 3-cm dish) and allowed to lay for 12 hr before removal and egg counts.

Immunofluorescence

Day 1 adult hermaphrodites were dissected in PBS/levamisole and fixed in 0.5% triton/1% paraformaldehyde for 5 min in a humid chamber. Slides were freeze-cracked and briefly immersed in methanol. Following fixation, slides were washed in PBST and incubated in primary antibody [α-RAD-51, kindly provided by Verena Jantsch, 1:5000; α-XND-1 (Wagner *et al.* 2010), 1:2000] overnight at 4°. Next day, slides were washed and incubated in secondary antibody (α-rabbit 568, 1:2000; α-guinea pig 633, 1:2000) for 2 hr at room temperature in the dark. Slides were mounted in Prolong Gold with DAPI (Life Technologies) and imaged on a Nikon A1r confocal microscope using a 63× Plan Fluor objective with 0.2-μm step sizes. Images were quantified using Volocity 3D software (PerkinElmer). RAD-51 foci were quantified by dividing the region from leptotene (transition zone) through the pachytene–diplotene border into six even zones (based on physical distance in micrometers) and individually scoring RAD-51 foci in each nucleus by scrolling through the images in the Z-dimension. RAD-51 counts were confirmed by examining 3D renderings of nuclei. Graphs represent the averages of three germlines for each genotype (Figure 3).

Yeast two- and three-hybrid plasmid construction

A population of predominately adult N2 hermaphrodites were washed three times in 1× M9 buffer, flash-frozen in RNAzol (Invitrogen), and stored at −80°. RNA was isolated by chloroform extraction and isopropanol precipitation and resuspended in DEPC water. Purity was verified by spectrophotometry. Complementary DNA (cDNA) synthesis was performed as described previously (Fukushige and Krause 2012). cDNA was diluted 1:15 in deionized water prior to further use.

Yeast two-hybrid (Y2H) plasmids were created from pGAD-C1 and pGBD-C1. The additional plasmid used in yeast three-hybrid (Y3H) analysis was created from pRS-ADH-416. pGAD-SWS-1 was synthesized by Genewiz (Gene Synthesis Services, South Plainfield, NJ) using codon-optimized sequences for expression in *S. cerevisiae*. pGBD-SWS-1 was created by subcloning SWS-1 into pGBD using 5′ *Sma*I and 3′ *Bgl*II restriction sites. SWIM domain mutants were made by site-directed mutagenesis of the pGAD-SWS-1 plasmid for SWS-1-C133S (SWS-1.C133S.F and SWS-1.C133S.R) and SWS-1-A156T (SWS-1.A156T.F and SWS-1.A156T.R) (Table S2). pGAD-RIP-1 and pGAD-RFS-1 were constructed using standard restriction digestion and ligation techniques. First, PCR amplification was used for the coding regions of both *rip-1* and *rfs-1* genes from N2 cDNA using oligonucleotide pairs RIP-1.F/RIP-1.R and RFS-1.F/RFS-1.R, respectively (Table S2). *rip-1* was subcloned into pGBD and pRS-ADH-416 using 5′ *Bam*HI and 3′ *Sal*I restriction sites. Walker B motif mutant was made by site-directed mutagenesis (RIP-1.D131A.F and RIP-1.D131A.R; Table S2) of pGBD-RIP-1. *rfs-1* was subcloned into pGBD using 5′ *Eco*RI and 3′ *Bgl*II restriction sites. All other plasmids were constructed as previously described (Godin *et al.* 2015).

Yeast two- and three-hybrid assays

Yeast strains, media, and yeast two-hybrid assays were performed as previously described (Godin *et al.* 2015) with the

following modifications. For Y2H analysis, pGAD and pGBD plasmids were cotransformed into the PJ69-4A Y2H strain (James *et al.* 1996) and 1 mM histidine competitive inhibitor, 3-amino-1,2,4-triazole (3AT), was used to detect more stringent Y2H interactions (SC−LEU−TRP−URA+3AT; Sigma Aldrich). For Y3H analysis, pGAD, pGBD, and pRS-ADH-416 (with URA selection marker) plasmids were cotransformed into the PJ69-4A Y2H strain. Yeast were selected for expression by growth on SC−LEU−TRP (Y2H) or SC−LEU−TRP−URA (Y3H) solid medium. Plates were grown for 2–4 days at 30° and photographed.

Data availability

Strains are available upon request. Supplemental Table S1 contains a list of all *C. elegans* strains generated in this study.

Results

sws-1 contributes to germline HR repair

We generated an *sws-1* allele using CRISPR/Cas9-mediated genome engineering (Figure 1, A and B, and *Materials and Methods*) (Dickinson *et al.* 2013; Arribere *et al.* 2014). Using this approach, we identified a founder strain with a 3-bp deletion/83-bp insertion in exon 2 just downstream of the predicted Cas9 cleavage site, designated as *ea12* (Figure 1, A and B, and Figure S1). Interestingly, the *dpy-10(cn64)* repair oligo donated most of the sequence for the insertion. *sws-1(ea12)* (hereafter referred to as *sws-1*) is predicted to produce the first 19 amino acids of the wild-type SWS-1 protein followed by 32 frameshifted amino acids prior to truncation (Figure 1C). Given the substantial truncation of the protein, including the conserved SWIM domain encoded in exon 4 (Figure 1A), and that disruption of the SWIM domain in *S. cerevisiae* Shu2 results in a nonfunctional protein (Godin *et al.* 2015), we expect *ea12* to be a null allele. Consistent with the presence of a premature stop codon, which triggers nonsense-mediated messenger RNA (mRNA) decay, we detect approximately fivefold less *sws-1* mRNA in *sws-1(ea12)* hermaphrodites compared to wild type (Figure 1D).

sws-1 homozygotes are viable, although they exhibit decreased survival compared to their wild-type counterparts ($P = 0.0399$, Mann–Whitney) (Table 1, rows B and C). This decrease in survival is not solely attributable to embryonic lethality, as we found that a small but significant percentage of *sws-1* homozygotes fail to develop past the L2 stage [$P < 0.001$ *vs.* wild type (wt), Fisher's exact test] (Figure 1E). We also observed a fourfold increase in male frequency compared to their wild-type counterparts ($P = 0.0114$, Mann–Whitney) (Table 1, rows B and C). These results suggest that *sws-1* is required for both normal development and X chromosome disjunction.

In other eukaryotes, such as *S. cerevisiae*, the Rad51 paralogs and a SWIM domain-containing protein form the Shu complex and share HR phenotypes (Shor *et al.* 2005; Mankouri *et al.* 2007). Therefore, we asked whether *sws-1* mutants would

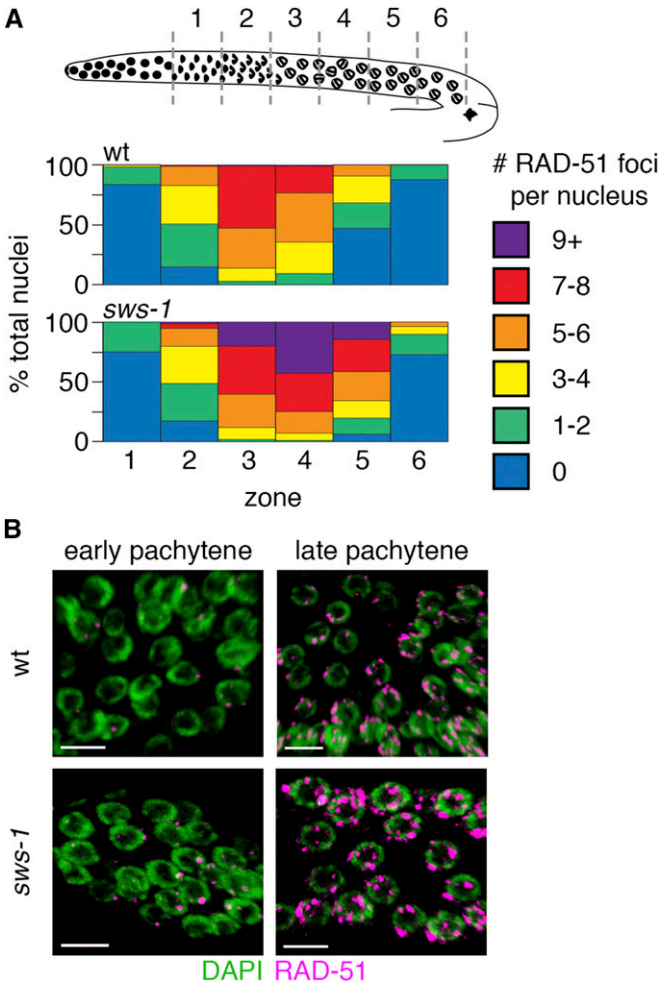

Figure 3 *sws-1* alters meiotic RAD-51 dynamics. (A) Quantitative analysis of RAD-51 foci during meiotic prophase. Diagram depicts organization of the hermaphrodite germline with meiotic prophase prior to diplotene divided into six equal-sized zones (gray dashed lines) based on physical distance. The heatmap shows the percentage of total nuclei per zone with the indicated number of RAD-51 foci from wild type (wt) (top) and *sws-1* (bottom) germlines (for color code, see legend). (B) Representative images of early and late pachytene nuclei in wt (top) and *sws-1* (bottom) showing higher levels of RAD-51 foci (magenta) on DNA (green). Bar, 5 μm.

exhibit similar phenotypes to RAD-51 paralog mutants in worms. In *C. elegans*, the two known RAD-51 paralogs, *rfs-1* and *rip-1*, confer reduced survival and *him* phenotypes (Ward *et al.* 2007; Yanowitz 2008; Taylor *et al.* 2015). Importantly, the reduced survival and *him* phenotypes of *sws-1* resembled those of *rfs-1* and *rip-1* (Table 1, rows D and F), suggesting that *sws-1* may have an analogous role in HR repair. To test this, we analyzed the viability and cytology of *helq-1;sws-1* double mutants. *helq-1* encodes a conserved DNA helicase that functions in HR-mediated repair during replication stress and meiosis (Muzzini *et al.* 2008; Ward *et al.* 2010). In meiosis, *helq-1* exhibits synthetic lethality with both *rfs-1* and *rip-1* due to persistent HR intermediates, suggesting that *helq-1* and *rfs-1/rip-1* perform overlapping roles in DSB repair (Ward *et al.* 2010; Taylor *et al.* 2015). Whereas *helq-1* single mutants

Table 2 Spontaneous revertant frequencies of *unc-58(e665)*

unc-58(e665) background	Trial	Plates with revertants/total plates	Mutation frequency ± SEM
Wild type	1	0/40	$7.06 \times 10^{-7} \pm 7.06 \times 10^{-7}$
	2	1/38	
	3	0/39	
	4	0/36	
sws-1	1	2/41	$2.00 \times 10^{-6} \pm 1.26 \times 10^{-6}$
	2	0/40	
	3	0/37	
	4	1/39	

unc-58 reversion assay was carried out as described in *Materials and Methods*. A plate was scored as having a reversion event if it contained wild-type moving worms. Mutation frequency was calculated by dividing the proportion of plates with reversion events by the number of haploid genomes per plate. The data are presented as the mean mutation frequency ± SEM for four trials.

exhibited low levels of lethality (~3.6%), *helq-1;sws-1* double mutants displayed ~63% lethality in the F_2 generation (Figure 2A). Analysis of diakinesis-stage nuclei in *helq-1;sws-1* hermaphrodites revealed chromatin abnormalities associated with impaired DSB repair—including decondensed chromatin, DNA fragments, and chromosome aggregates—in nearly all nuclei scored (Figure 2, B and C). The redundancy with *helq-1* indicates that *sws-1* functions in HR repair and raises the possibility that *sws-1* functions with the RAD-51 paralogs in this role.

We reasoned that, if *sws-1* is required for HR repair during meiosis, we might observe a change in RAD-51 dynamics compared to wild type. We quantified RAD-51 foci in wild-type and *sws-1* germlines from the onset of leptotene [transition zone (TZ)] through pachytene, the time at which SPO-11-induced DSB breaks are made and repaired (Figure 3). In wild-type germlines, RAD-51 foci first appear in the TZ, peak during early pachytene and then disappear by late pachytene as HR progresses (Alpi *et al.* 2003) (Figure 3, wt). Similar to wild type, most *sws-1* nuclei had no RAD-51 foci upon entry to meiosis (Figure 3, zone 1), and RAD-51 foci slowly accumulated as nuclei progressed into pachytene. However, in later stages of pachytene, a greater proportion of *sws-1* nuclei had seven or more RAD-51 foci than their wild-type counterparts (Figure 3A, $P < 0.05$ for seven to eight foci in zone 3, $P < 0.0001$ for more than nine foci in zone 3, $P < 0.05$ for more than nine foci in zone 4, Student's *t*-test). Although this may be explained by increased formation of DSBs, the exclusively late-pachytene persistence of RAD-51 foci suggests that *sws-1* nuclei were delayed in removing RAD-51 foci. At the late-pachytene–diplotene border, the proportion of nuclei containing RAD-51 foci was again similar to wild type (Figure 3, zone 6), indicating that all DSBs are eventually repaired.

The observation that RAD-51 foci eventually resolve in *sws-1* germlines (Figure 2B and Figure 3A) left us curious about the cause of lethality in *sws-1* mutants. *C. elegans* exhibits strong CO control such that only one DSB per chromosome pair becomes an interhomolog CO (Barnes *et al.* 1995; Meneely *et al.* 2002; Hillers and Villeneuve 2003). One possible explanation for the lethality, then, is that *sws-1* mutants are deficient in HR repair of DSBs not designated to be repaired as interhomolog COs. To test this hypothesis, we analyzed the competency of *sws-1* mutants for intersister HR by examining the cytology of diakinesis-stage oocytes in *syp-3;sws-1* double mutants (Figure S2). *syp-3* is a component of the synaptonemal complex (SC) that holds homologs together during meiosis. In the absence of the SC, HR repair between homologous chromosomes cannot occur, and DSBs are repaired from the sister chromatids. Consequently, *syp-3* mutants exhibit an average of 11.6 condensed DAPI-staining bodies at diakinesis (Figure S2) (Smolikov *et al.* 2007a,b). We did not observe a significant change in either number or morphology of DAPI-staining bodies at diakinesis between *syp-3* and *syp-3;sws-1* mutants (Figure S2), suggesting that *sws-1* mutants are competent for intersister HR.

A second possibility is that *sws-1* mutants have an increased reliance on error-prone DSB repair pathways. If this is the case, *sws-1* might be expected to show an increase in spontaneous mutation rate, which can be assessed by the reversion to wild-type movement of *unc-58(e665)*, a missense gain-of-function mutation that confers paralysis (Harris *et al.* 2006). Although not significantly different from controls, *sws-1;unc-58* mutants exhibited a trend toward increased mutation rate with an approximately threefold increase in reversion to non-Unc offspring compared to *unc-58* alone (Table 2, $P = 0.4058$, Student's *t*-test). These observations are consistent with what has been reported for *rfs-1* mutants (Yanowitz 2008) and may suggest that HR factors are not critical for correction of mismatches during DNA replication. However, HR factors, including *rfs-1*, have been shown to be important for maintaining the integrity of poly-G/C tracts in the absence of the helicase *dog-1*, which prevents the formation of deletions in G/C-rich DNA by unwinding secondary DNA structures that hinder replication fork progression (Cheung *et al.* 2002; Youds *et al.* 2006; Ward *et al.* 2007). We observed increased deletion frequency in *dog-1;sws-1* mutants compared to *dog-1* alone (Figure 4, $P = 0.0386$, Fisher's exact test), suggesting increased reliance on mutagenic repair pathways in the absence of *sws-1*. Collectively, these results suggest that *sws-1* functions in HR and is important for maintaining genome integrity during DNA replication.

sws-1 mutants are sensitive to genotoxins that induce HR substrates

In *C. elegans*, both *rfs-1* and *rip-1* mutants display sensitivity to DSB-inducing agents, especially those that obstruct

replication fork progression (Ward *et al.* 2007; Taylor *et al.* 2015). To further investigate the role of *sws-1* in HR repair, we exposed hermaphrodites to a subset of genotoxins that create HR repair substrates: IR, MMS, HU, or CPT. The survival of the offspring laid post exposure reflects the repair capacity in the hermaphrodite germline. As shown in Figure 5, we observed a modest, but statistically significant, increased sensitivity of *sws-1* mutants to IR, MMS, and HU compared to their wild-type counterparts (Figure 5, A–C). By contrast, *sws-1* mutants were dramatically more sensitive than wild type to CPT (Figure 5D). The reduced progeny survival following CPT treatment was accompanied by a twofold increase in apoptotic germline nuclei (Figure S3), indicating that *sws-1* meiotic nuclei were unable to repair CPT-induced DSBs. This increased sensitivity to CPT may suggest that *sws-1* plays a more prominent role in the repair of a specific subset of DSB-inducing lesions.

The *S. cerevisiae* Shu complex has been shown *in vitro* to promote Rad51-mediated repair in concert with Rad52 and the Rad55-Rad57 heterodimer by stimulating Rad51 loading onto ssDNA and stabilizing it thereafter (Gaines *et al.* 2015). Further studies in *S. cerevisiae* suggest that the Shu complex promotes Rad51 assembly on meiotic chromosomes *in vivo* based on a reduced number of Rad51 foci in Shu complex mutants (Sasanuma *et al.* 2013). In *C. elegans*, the RAD-51 paralogs, *rfs-1* and *rip-1*, stabilize RAD-51 foci in response to cisplatin, nitrogen mustard, and UV (Ward *et al.* 2007; Taylor *et al.* 2015). We reasoned that the increased sensitivity of *sws-1* mutants to CPT may stem from a failure to stabilize RAD-51 presynaptic filaments at damage sites. To test this hypothesis, we visualized RAD-51 foci by immunofluorescence (Figure 6). In wild-type and *sws-1* germline nuclei under normal conditions, RAD-51 foci were rarely, if at all, seen in the mitotic zone (Figure 6A). In response to CPT treatment, RAD-51 foci were readily visible throughout the mitotic zone nuclei in wild-type germlines, indicative of ongoing HR repair (compare Figure 6, A and C). In contrast, we observed a striking absence of RAD-51 foci in the mitotic zone of *sws-1* germlines following CPT exposure (compare Figure 6, B and D). These results suggest that the sensitivity of *sws-1* mutants to CPT may be due to a failure to undergo HR repair.

RIP-1 interacts with SWS-1 by yeast two-hybrid and bridges an interaction between SWS-1 and RFS-1 by yeast three-hybrid

The HR repair defects of *sws-1* mutants, including synthetic lethality with *helq-1*, resemble those of the RAD-51 paralogs *rfs-1* and *rip-1* (Ward *et al.* 2007, 2010; Taylor *et al.* 2015). To further explore if these factors act in the same pathway, we compared the lethality and male frequency of double- and triple-mutant combinations of *sws-1*, *rfs-1*, and *rip-1* (Table 1, rows C–I). We observed that the incidence of lethality was statistically unchanged between the *rfs-1,rip-1;sws-1* triple mutant and any of the single mutants (ANOVA, $P > 0.05$). Curiously, the lethality of *rip-1;sws-1* double mutants exhibited reduced lethality compared to the *rfs-1,rip-1;sws-1* triple mutant ($P < 0.05$, Tukey's test, Table S3), although there was no statistical difference in lethality between *rip-1;sws-1* and either *rfs-1;sws-1* or *rfs-1,rip-1* double mutants. Furthermore, the lethality of the *rfs-1,rip-1;sws-1* triple mutant is well below the additive value predicted from each single mutant, suggesting that the cause of lethality is shared. The male frequency of *rfs-1,rip-1;sws-1* triple mutants was unchanged from either *rfs-1* or *rip-1* single mutants, but significantly increased compared to *sws-1* single mutants ($P < 0.05$, Tukey's test, Table S4). This result is consistent with the observation in yeast that *psy3* or *csm2* mutants exhibit more severe phenotypes compared to *shu1* or *shu2* mutants (Sasanuma *et al.* 2013; Godin *et al.* 2015) and highlights the importance of the RAD-51 paralogs in Shu complex function.

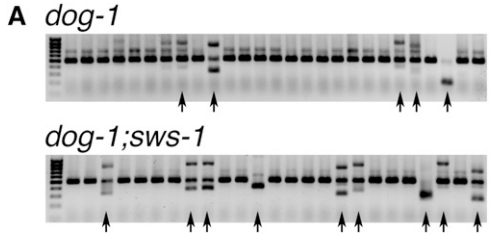

B

	n	# animals with deletions
wt	95	0
sws-1	96	1
dog-1	191	35
dog-1;sws-1	192	53*

Figure 4 *sws-1* maintains G/C tract stability in the absence of *dog-1*. (A) Amplification of the *vab-1* G/C tract in *dog-1* (top) and *dog-1;sws-1* (bottom) mutants. Deletions in the amplified region are observed as faster-migrating bands on a 1.5% agarose gel (black arrows). (B) Quantification of deletion frequency in wild type (wt), *sws-1*, *dog-1*, and *dog-1;sws-1* mutants. Number of individual animals with one or more deletions in the *vab-1* G/C tract as described in A are indicated. *$P < 0.05$, Fisher's exact test.

In yeast and human cells, Shu2/SWS1 is found in complexes with the Rad51 paralogs Csm2-Psy3 and SWSAP1, respectively (Martin *et al.* 2006; Liu *et al.* 2011; Godin *et al.* 2013, 2015). To determine if SWS-1 similarly interacts with the known RAD-51 paralogs in *C. elegans*, we performed Y2H analysis, fusing SWS-1, RFS-1, or RIP-1 to the GAL4 activation domain (pGAD) and the GAL4 DNA-binding domain (pGBD). By Y2H, SWS-1 interacted directly with RIP-1 but not RFS-1 in both configurations (Figure 7A and Figure S4). Since yeast Shu2 interacts with the other Shu complex members Shu1 and Psy3, and human SWS1 directly interacts with SWSAP1, we next examined if worm SWS-1 could interact with any other member of the yeast Shu complex or with human SWSAP1 by Y2H. We were unable to detect a cross-species Y2H interaction between worm SWS-1 and the other yeast or human Shu complex members (Figure S5 and data not shown). These data make it unlikely that the yeast Shu complex members are bridging an interaction between SWS-1 and RIP-1.

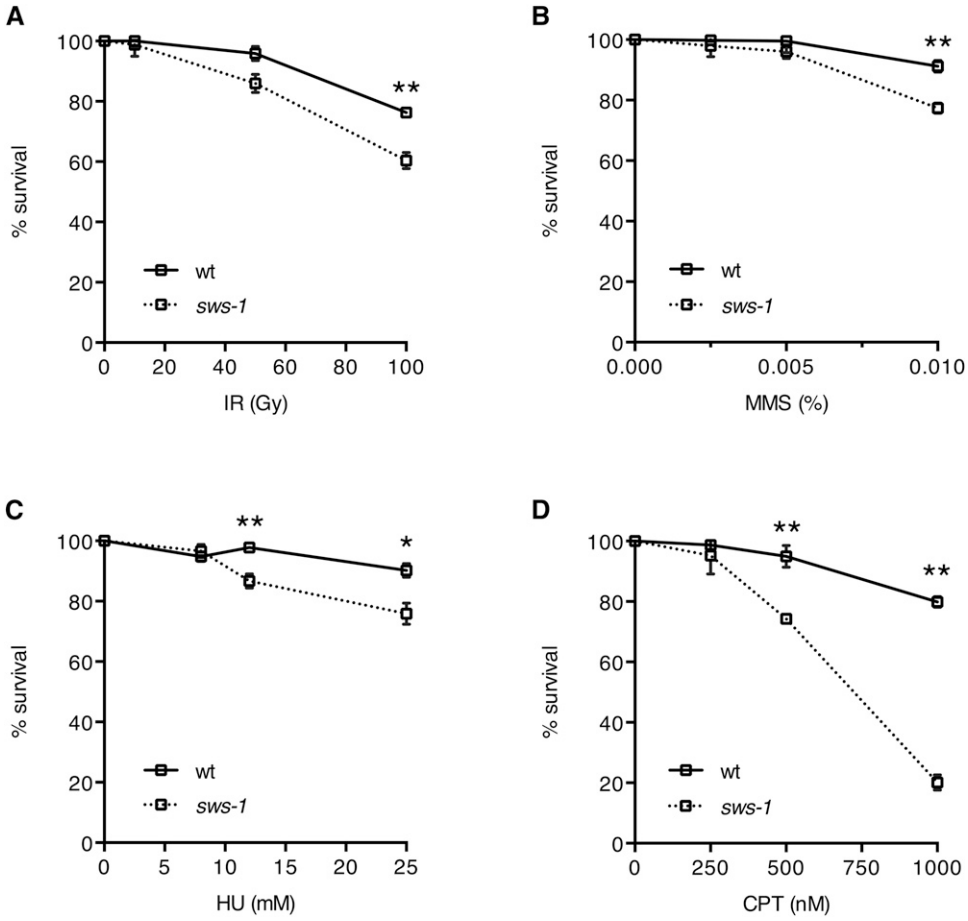

Figure 5 *sws-1* mutants are sensitive to genotoxins that induce HR repair substrates. Progeny survival of hermaphrodites treated with IR (A), MMS (B), HU (C), or CPT (D) as described in *Materials and Methods*. Survival was calculated as the number of adult progeny divided by the number of eggs and L1's relative to untreated worms ± SEM from at least 22 adults over two trials. Statistical analysis was performed using Student's *t*-test (*$P < 0.01$, **$P < 0.0001$).

Rather, these data support the conclusion that SWS-1 and RIP-1 directly interact and comprise core components of the worm Shu complex.

Based on the known Y2H interaction between RIP-1 and RFS-1 (Taylor *et al.* 2015) (Figure 7A), we hypothesized that RIP-1 may bridge an interaction between SWS-1 and RFS-1.

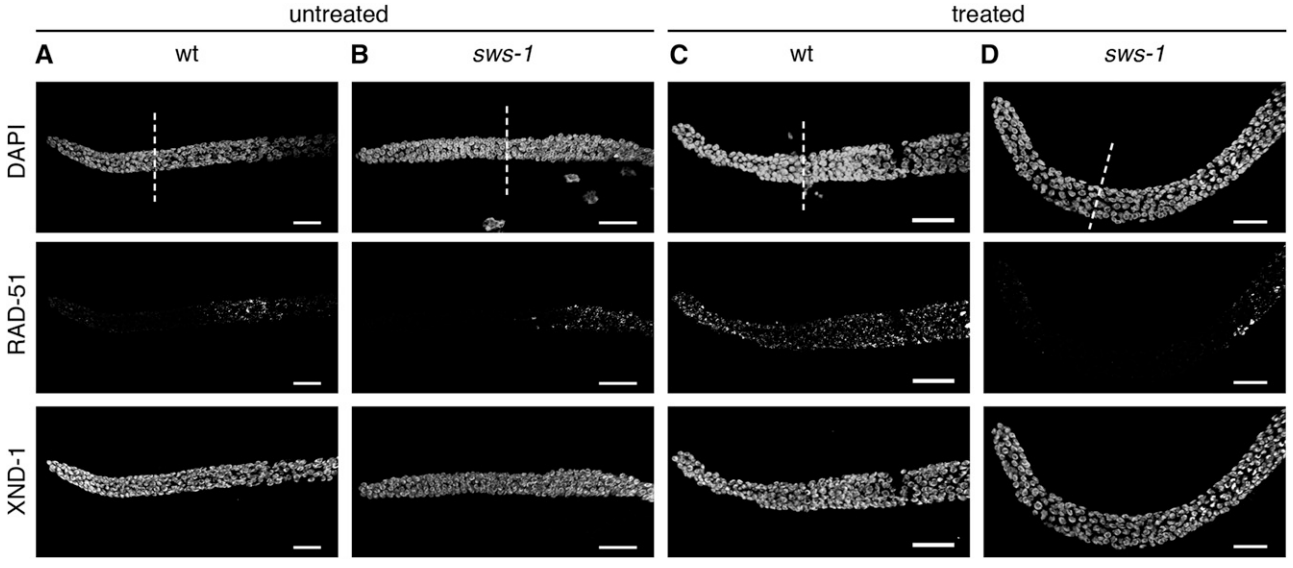

Figure 6 *sws-1* fails to form mitotic RAD-51 foci following CPT treatment. Immunofluorescence of RAD-51 with or without CPT exposure in germlines of wild type (wt) (A and C) and *sws-1* (B and D) hermaphrodites. Treated worms were exposed to 500 nM CPT as described in *Materials and Methods* and dissected at the end of the recovery period. Immunostaining conditions are described in *Materials and Methods*. White dashed line marks the beginning of transition zone. XND-1 immunofluorescence serves as a staining control. Bar, 20 μm.

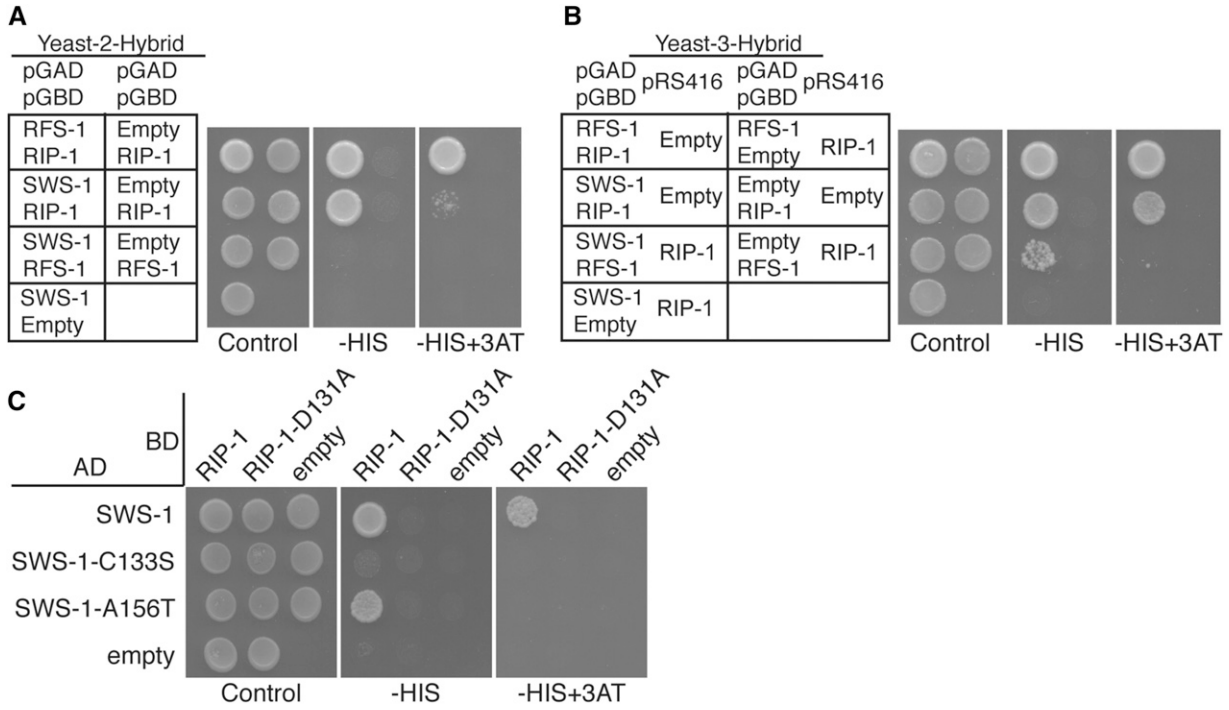

Figure 7 RIP-1 interacts with SWS-1 and bridges an interaction between SWS-1 with RFS-1. Y2H (A and C) and Y3H (B) from left to right show plating controls on SC−LEU−TRP or SC−LEU−TRP−URA, respectively, with the additional dropout of histidine (−HIS) and histidine with 3-amino-1,2,4-triazole (−HIS+3AT), indicating a Y2H or Y3H interaction. Within each panel, the left column shows potential interactions between two proteins and the right column shows an empty vector control. RIP-1 interacts with both SWS-1 and RFS-1. SWS-1 and RFS-1 do not interact (A). With constitutive expression of RIP-1, SWS-1 and RFS-1 promote growth on SC−LEU−TRP− URA−HIS, indicating a Y3H interaction (row 3 in B). Two SWIM domain mutations were created in SWS-1, C133S, and A156T. SWS-1-C133S disrupts interaction with RIP-1 (row 2 in C). SWS-1-A156T decreases interaction with RIP-1 on –HIS+3AT (row 3 in C). A Walker B motif mutation that disrupts interaction with SWS-1, SWS-1-C133S, and SWS-1-A146T (column 2 in C) was introduced into RIP-1.

To test this possibility, we performed a Y3H assay in which SWS-1 was again expressed as a fusion with the GAL4 activation domain and RFS-1 as a fusion with the GAL4 DNA-binding domain, but in this case a third, untagged, vector expressing RIP-1 or an empty vector was coexpressed (pRS416-RIP-1 or pRS416, respectively) (Figure 7B). By Y3H, we find that in the presence of RIP-1, but not the empty vector control, SWS-1 and RFS-1 confer growth on the Y3H medium, suggesting that these proteins are now able to interact (Figure 7B). Together, these studies suggest that RIP-1 facilitates ternary complex formation with SWS-1 and RFS-1.

SWIM domain in SWS-1 and the Walker B motif in RIP-1 are important for their yeast two-hybrid interaction

We originally identified SWS-1 because of its invariant SWIM domain, a zinc-finger-binding-like motif (CxCxnCxHxxA, "n" being 6–25 residues), which we found to be important for Sws1 protein family Y2H interactions with the Rad51 paralogs in yeast and humans (Godin *et al.* 2015). Therefore, we wondered whether the SWIM domain of SWS-1 would be important for its interaction with RIP-1. We mutated the second cysteine of the SWIM domain to serine (*sws-1-C133S*) in the Y2H expression vector and retested the functionality of this protein to support growth on SC−HIS medium or the more stringent SC−HIS+3AT medium, where 3AT is a competitive inhibitor of histidine. As shown in Figure 5, *sws-1-C133S* abrogated the Y2H interaction between SWS-1 and RIP-1 (Figure 7C). Previously, we identified a cancer-associated mutation in human SWS1 on the COSMIC database where the invariant alanine was mutated to a threonine (Godin *et al.* 2015). Therefore, we made the analogous mutation in SWS-1 and found that *sws-1-A156T* maintains its interaction with RIP-1 at lower stringencies but exhibited reduced Y2H interaction upon more stringent conditions (Figure 7C; plating on SC–HIS medium *vs.* SC–HIS+3AT). Together, these results suggest that the SWIM domain in SWS-1 is important for its interaction with RIP-1.

RIP-1 is defined as a RAD51 paralog by the presence of a conserved Walker B-like motif. Therefore, we next asked whether the Walker B motif is important for its interaction with SWS-1. By Y2H, expression of a RIP-1 Walker B mutant, *rip-1-D131A*, disrupts interaction with both wild-type SWS-1 and the SWS-1 SWIM domain mutants (C133S and A156T) (Figure 7C). Interestingly, *rip-1-D131A* was found to maintain its Y2H interaction with RFS-1 under the same conditions (Taylor *et al.* 2015). Therefore, RIP-1 interacts with SWS-1 through its Walker-B-like motif.

Discussion

SWS-1 functions in HR with RFS-1 and RIP-1

C. elegans sws-1 was identified as a putative Shu2 homolog based on the presence of a conserved SWIM domain,

although no functional analysis was performed (Godin *et al.* 2015). Using a nonsense allele of *sws-1* (Figure 1), we show that *sws-1* is involved in HR in the germline. *sws-1* mutants exhibit mild reduction in viability and increased male frequency compared to wild type (Table 1) The mildness of these *sws-1* phenotypes belies its importance when worms are further compromised by loss of *helq-1*. *helq-1*; *sws-1* double mutants exhibit synthetic lethality and diakinesis oocytes with severe chromosomal abnormalities (Figure 2). These results indicate functional redundancy of *sws-1* and *helq-1* for meiotic HR repair. Impaired meiotic HR functions become obvious in *sws-1* single mutants based on the sensitivity to DSB-inducing agents and, perhaps most significantly, increased accumulation of RAD-51 in mid-late pachytene nuclei.

The clear substrate preference for SWS-1 at replication forks implicates a mitotic role: first, *sws-1* is needed to maintain poly-G/C tract stability in the absence of *dog-1* (Figure 4), which is predicted to function during DNA replication (Youds *et al.* 2006); second, *sws-1* mutants are most sensitive to CPT, which induces DSBs by blocking replication forks (Figure 5); third, RAD-51 foci were notably absent in *sws-1* mitotic nuclei following CPT treatment (Figure 6). However, the timing of our genotoxin exposure assays is consistent with assessing repair capacity of meiotic nuclei (Jaramillo-Lambert *et al.* 2007; Kessler and Yanowitz 2014). Consistent with this, we observed a two- and fourfold increase in germline apoptosis following treatment with CPT in *sws-1* and *rfs-1* hermaphrodites, respectively (Figure S3). Collectively, these results suggest that *sws-1* promotes HR by stabilizing RAD-51 at specific HR substrates in both mitosis and meiosis, as has been shown for *rfs-1* and *rip-1* (Ward *et al.* 2007; Taylor *et al.* 2015). Using this cell biological approach, we cannot distinguish if SWS-1 promotes RAD-51 loading or stabilizes RAD-51 after it has loaded onto ssDNA, as previous work with RFS-1 and RIP-1 has suggested (Taylor *et al.* 2015).

The similar phenotypes of *sws-1* and the RAD-51 paralogs *rfs-1* and *rip-1* (Ward *et al.* 2007, 2010; Taylor *et al.* 2015) prompted us to examine whether these genes function together in HR repair. The lack of additive lethality among double- and triple-mutant combinations strongly suggests that they function together (Table 1 and Table S3). In support of this notion, we observe a direct interaction between SWS-1 with RIP-1 and RFS-1 by Y2H (Figure 7). Taken together, our results suggest that SWS-1, RIP-1, and RFS-1 form a conserved complex to promote RAD-51-dependent HR (Figure 8). We note that *rfs-1* mutants have a higher male frequency than *sws-1*, which likely contributes to the increased male frequency in the triple mutants (Table 1 and Table S4). While we cannot rule out that *rfs-1* may have additional roles outside of the Shu complex, it may be that mutation of *rfs-1* may have more severe consequences than other members of the complex because it directly mediates an interaction with RAD-51 (Ward *et al.* 2010; Taylor *et al.* 2015).

C. elegans Shu complex is composed of SWS-1, RIP-1, and RFS-1

Budding and fission yeast as well as the human Shu complexes have been defined as consisting of an SWS1 protein family member and its associated RAD51 paralog interacting partners (Shor *et al.* 2005; Martin *et al.* 2006; Liu *et al.* 2011). Using this definition, we propose that *C. elegans* contains a Shu complex composed of SWS-1, RIP-1, and RFS-1 (Figure 8). Previously, we have shown that yeast Shu2 is most closely related to SWS-1 in *C. elegans* using sequence homology to the conserved SWIM domain; however, it remained unknown whether this conservation was limited to its sequence or if it extended to SWS-1 protein function (Godin *et al.* 2015). Given the embryonic lethality observed in the knockout models of the mouse RAD51 paralogs (Deans *et al.* 2000; Thacker 2005; Kuznetsov *et al.* 2009; Suwaki *et al.* 2011), our work in *C. elegans* provides a unique opportunity to study Shu complex disruption in a multicellular organism. Here we demonstrate the first evidence for a functional worm Shu complex consisting of SWS-1 and RIP-1, which likely directly interact through the SWIM domain of SWS-1 and the Walker B motif of RIP-1. Note that it is possible that the *sws-1* SWIM domain mutants may not be properly folded or expressed. Additionally, RIP-1 bridges an interaction between SWS-1 and RFS-1 (Figure 7 and Figure 8). Unlike yeast and humans, only two RAD-51 paralogs have been identified in worms (Ward *et al.* 2007; Taylor *et al.* 2015). One possibility is that the worm RAD-51 paralogs RFS-1 and RIP-1 are sufficient to perform all the various functions of the RAD-51 paralogs described in other eukaryotes. Alternatively, additional RAD-51 paralogs have yet to be identified in *C. elegans*. Importantly, the budding yeast Csm2 and Psy3 proteins were shown to be Rad51

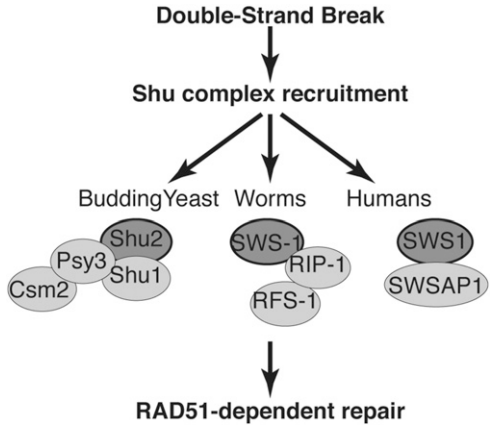

Figure 8 Model of Shu complex function in promoting Rad51-mediated repair. After a double-strand break occurs, the Shu complex in budding yeast, worms, or humans is recruited to sites of DNA damage where it subsequently promotes RAD51-dependent repair. In budding yeast, the Shu complex is composed of a SWIM domain containing protein, Shu2, the Rad51 paralogs Csm2-Psy3, and Shu1. In humans the exact components of the Shu complex are not completely known but consist of the SWIM-domain-containing protein SWS1 and its associated RAD51 paralog SWSAP1. Here we define the worm Shu complex to consist of SWS-1 and the RAD-51 paralogs RFS-1 and RIP-1, where SWS-1 directly interacts with RIP-1 through the SWIM domain of SWS-1 and the Walker-B motif of RIP-1. RIP-1 bridges an interaction between SWS-1 and RFS-1, suggesting that it can interact with both proteins simultaneously. SWS1 family members are depicted by dark gray circles with a black outline and the other Shu complex components by light gray circles.

paralogs only upon crystallization as their sequence conservation to Rad51 is extremely poor (She *et al.* 2012; Tao *et al.* 2012; Sasanuma *et al.* 2013). Furthermore, the poor sequence conservation of Rad51 paralogs between species and our inability to complement yeast harboring disruptions of the Shu complex genes with worm proteins also makes direct comparisons between the individual Rad51 paralogs challenging (data not shown). Therefore, further studies will be important for determining whether additional RAD-51 paralogs exist in worms and which RAD-51 paralogs correlate with the functions attributed to the equivalent human and yeast proteins.

Substrate specificity of the worm Shu complex

We find that *sws-1* mutants are most sensitive to the DNA-damaging agent camptothecin (Figure 5). In contrast, budding yeast containing a deletion of the *sws-1* ortholog *shu2Δ* exhibits a more pronounced sensitivity to MMS (Shor *et al.* 2005; Mankouri *et al.* 2007; Ball *et al.* 2009). Therefore, it is possible that the different DNA damage sensitivities observed for the Shu complex members relative to other more general HR factors may indicate a specialized role of SWS-1 in repair of specific types of DNA lesions. Camptothecin is a topoisomerase I inhibitor that would specifically become covalently modified on the ssDNA end and would therefore be converted into a DSB upon replication fork progression. It is intriguing to speculate that perhaps the specific sensitivity of *sws-1* worms to camptothecin provides a framework for determining the types of DNA structures created during meiosis. Studies in yeast have shown that the Shu complex is important for driving homolog bias during meiosis, where the homologous chromosome is made the preferred partner for repair over the sister chromatid (Hong and Kim 2013; Hong *et al.* 2013; Sasanuma *et al.* 2013). Therefore, additional mechanistic studies are needed to identify the preferred substrates for the Shu complex in both mitotic and meiotic repair. Importantly, our work on the worm Shu complex provides a new way in which to study disruption in the Shu complex in the context of a multicellular organism that will help us to determine why mutations in the human RAD51 paralogs are associated with cancer predisposition and in some cases Fanconi anemia.

Acknowledgments

We thank Tyler Machovina for performing injections and initial screening; Simon Boulton, Ann Rose, and Sarit Smolikov for strains; Verena Jantsch for the anti-RAD-51 antibody; and Francis Gandhi for guidance with qPCR. Some strains were provided by the *Caenorhabditis* Genetics Center, which is funded by National Institutes of Health (NIH) Office of Research Infrastructure Programs (P40 OD010440). Sequencing of CRISPR constructs and of *sws-1* was performed in the Genomics Research Core at the University of Pittsburgh. This work was supported by NIH grants to K.B. (ES024872) and J.Y. (GM1040070).

Literature Cited

Alpi, A., P. Pasierbek, A. Gartner, and J. Loidl, 2003 Genetic and cytological characterization of the recombination protein RAD-51 in Caenorhabditis elegans. Chromosoma 112: 6–16.

Arribere, J. A., R. T. Bell, B. X. Fu, K. L. Artiles, P. S. Hartman *et al.*, 2014 Efficient marker-free recovery of custom genetic modifications with CRISPR/Cas9 in *Caenorhabditis elegans*. Genetics 198: 837–846.

Ball, L. G., K. Zhang, J. A. Cobb, C. Boone, and W. Xiao, 2009 The yeast Shu complex couples error-free post-replication repair to homologous recombination. Mol. Microbiol. 73: 89–102.

Barnes, T. M., Y. Kohara, A. Coulson, and S. Hekimi, 1995 Meiotic recombination, noncoding DNA and genomic organization in *Caenorhabditis elegans*. Genetics 141: 159–179.

Brenner, S., 1974 The genetics of *Caenorhabditis elegans*. Genetics 77: 71–94.

Cheung, I., M. Schertzer, A. Rose, and P. M. Lansdorp, 2002 Disruption of dog-1 in Caenorhabditis elegans triggers deletions upstream of guanine-rich DNA. Nat. Genet. 31: 405–409.

Cole, F., S. Keeney, and M. Jasin, 2010 Evolutionary conservation of meiotic DSB proteins: more than just Spo11. Genes Dev. 24: 1201–1207.

Craig, A. L., S. C. Moser, A. P. Bailly, and A. Gartner, 2012 Methods for studying the DNA damage response in the Caenorhabdatis elegans germ line. Methods Cell Biol. 107: 321–352.

Deans, B., C. S. Griffin, M. Maconochie, and J. Thacker, 2000 Xrcc2 is required for genetic stability, embryonic neurogenesis and viability in mice. EMBO J. 19: 6675–6685.

Dickinson, D. J., J. D. Ward, D. J. Reiner, and B. Goldstein, 2013 Engineering the Caenorhabditis elegans genome using Cas9-triggered homologous recombination. Nat. Methods 10: 1028–1034.

Fukushige, T., and M. Krause, 2012 Myogenic conversion and transcriptional profiling of embryonic blastomeres in Caenorhabditis elegans. Methods 56: 50–54.

Gaines, W. A., S. K. Godin, F. F. Kabbinavar, T. Rao, A. P. VanDemark *et al.*, 2015 Promotion of presynaptic filament assembly by the ensemble of S. cerevisiae Rad51 paralogues with Rad52. Nat. Commun. 6: 7834.

Godin, S., A. Wier, F. Kabbinavar, D. S. Bratton-Palmer, H. Ghodke *et al.*, 2013 The Shu complex interacts with Rad51 through the Rad51 paralogues Rad55-Rad57 to mediate error-free recombination. Nucleic Acids Res. 41: 4525–4534.

Godin, S. K., C. Meslin, F. Kabbinavar, D. S. Bratton-Palmer, C. Hornack *et al.*, 2015 Evolutionary and functional analysis of the invariant SWIM domain in the conserved Shu2/SWS1 protein family from *Saccharomyces cerevisiae* to *Homo sapiens*. Genetics 199: 1023–1033.

Harris, J., M. Lowden, I. Clejan, M. Tzoneva, J. H. Thomas *et al.*, 2006 Mutator phenotype of *Caenorhabditis elegans* DNA damage checkpoint mutants. Genetics 174: 601–616.

Heyer, W. D., 2015 Regulation of recombination and genomic maintenance. Cold Spring Harb. Perspect. Biol. 7: a016501.

Hillers, K. J., and A. M. Villeneuve, 2003 Chromosome-wide control of meiotic crossing over in C. elegans. Curr. Biol. 13: 1641–1647.

Hodgkin, J., H. R. Horvitz, and S. Brenner, 1979 Nondisjunction mutants of the nematode *Caenorhabditis elegans*. Genetics 91: 67–94.

Hong, S., and K. P. Kim, 2013 Shu1 promotes homolog bias of meiotic recombination in Saccharomyces cerevisiae. Mol. Cells 36: 446–454.

Hong, S., Y. Sung, M. Yu, M. Lee, N. Kleckner *et al.*, 2013 The logic and mechanism of homologous recombination partner choice. Mol. Cell 51: 440–453.

Hoogewijs, D., K. Houthoofd, F. Matthijssens, J. Vandesompele, and J. R. Vanfleteren, 2008 Selection and validation of a set of reliable reference genes for quantitative sod gene expression analysis in C. elegans. BMC Mol. Biol. 9: 9.

James, P., J. Halladay, and E. A. Craig, 1996 Genomic libraries and a host strain designed for highly efficient two-hybrid selection in yeast. Genetics 144: 1425–1436.

Jaramillo-Lambert, A., M. Ellefson, A. M. Villeneuve, and J. Engebrecht, 2007 Differential timing of S phases, X chromosome replication, and meiotic prophase in the C. elegans germ line. Dev. Biol. 308: 206–221.

Jasin, M., and R. Rothstein, 2013 Repair of strand breaks by homologous recombination. Cold Spring Harb. Perspect. Biol. 5: a012740.

Karpenshif, Y., and K. A. Bernstein, 2012 From yeast to mammals: recent advances in genetic control of homologous recombination. DNA Repair (Amst.) 11: 781–788.

Keeney, S., C. N. Giroux, and N. Kleckner, 1997 Meiosis-specific DNA double-strand breaks are catalyzed by Spo11, a member of a widely conserved protein family. Cell 88: 375–384.

Kessler, Z., and J. Yanowitz, 2014 Methodological considerations for mutagen exposure in C. elegans. Methods 68: 441–449.

Krejci, L., V. Altmannova, M. Spirek, and X. Zhao, 2012 Homologous recombination and its regulation. Nucleic Acids Res. 40: 5795–5818.

Kuznetsov, S. G., D. C. Haines, B. K. Martin, and S. K. Sharan, 2009 Loss of Rad51c leads to embryonic lethality and modulation of Trp53-dependent tumorigenesis in mice. Cancer Res. 69: 863–872.

Lant, B., and W. B. Derry, 2014 Fluorescent visualization of germline apoptosis in living Caenorhabditis elegans. Cold Spring Harb. Protoc. 2014: 420–427.

Liu, T., L. Wan, Y. Wu, J. Chen, and J. Huang, 2011 hSWS1.SWSAP1 is an evolutionarily conserved complex required for efficient homologous recombination repair. J. Biol. Chem. 286: 41758–41766.

Makarova, K. S., L. Aravind, and E. V. Koonin, 2002 SWIM, a novel Zn-chelating domain present in bacteria, archaea and eukaryotes. Trends Biochem. Sci. 27: 384–386.

Mankouri, H. W., H. P. Ngo, and I. D. Hickson, 2007 Shu proteins promote the formation of homologous recombination intermediates that are processed by Sgs1-Rmi1-Top3. Mol. Biol. Cell 18: 4062–4073.

Martin, V., C. Chahwan, H. Gao, V. Blais, J. Wohlschlegel *et al.*, 2006 Sws1 is a conserved regulator of homologous recombination in eukaryotic cells. EMBO J. 25: 2564–2574.

Meneely, P. M., A. F. Farago, and T. M. Kauffman, 2002 Crossover distribution and high interference for both the X chromosome and an autosome during oogenesis and spermatogenesis in *Caenorhabditis elegans*. Genetics 162: 1169–1177.

Miller, K. A., D. M. Yoshikawa, I. R. McConnell, R. Clark, D. Schild *et al.*, 2002 RAD51C interacts with RAD51B and is central to a larger protein complex in vivo exclusive of RAD51. J. Biol. Chem. 277: 8406–8411.

Muzzini, D. M., P. Plevani, S. J. Boulton, G. Cassata, and F. Marini, 2008 Caenorhabditis elegans POLQ-1 and HEL-308 function in two distinct DNA interstrand cross-link repair pathways. DNA Repair (Amst.) 7: 941–950.

Paix, A., Y. Wang, H. E. Smith, C. Y. Lee, D. Calidas *et al.*, 2014 Scalable and versatile genome editing using linear DNAs with microhomology to Cas9 Sites in *Caenorhabditis elegans*. Genetics 198: 1347–1356.

Prakash, R., Y. Zhang, W. Feng, and M. Jasin, 2015 Homologous recombination and human health: the roles of BRCA1, BRCA2, and associated proteins. Cold Spring Harb. Perspect. Biol. 7: a016600.

Sasanuma, H., M. S. Tawaramoto, J. P. Lao, H. Hosaka, E. Sanda *et al.*, 2013 A new protein complex promoting the assembly of Rad51 filaments. Nat. Commun. 4: 1676.

Schmittgen, T. D., and K. J. Livak, 2008 Analyzing real-time PCR data by the comparative C(T) method. Nat. Protoc. 3: 1101–1108.

She, Z., Z. Q. Gao, Y. Liu, W. J. Wang, G. F. Liu *et al.*, 2012 Structural and SAXS analysis of the budding yeast SHU-complex proteins. FEBS Lett. 586: 2306–2312.

Shor, E., J. Weinstein, and R. Rothstein, 2005 A genetic screen for top3 suppressors in *Saccharomyces cerevisiae* identifies SHU1, SHU2, PSY3, and CSM2: four genes involved in error-free DNA repair. Genetics 169: 1275–1289.

Smolikov, S., A. Eizinger, A. Hurlburt, E. Rogers, A. M. Villeneuve *et al.*, 2007a Synapsis-defective mutants reveal a correlation between chromosome conformation and the mode of double-strand break repair during *Caenorhabditis elegans* meiosis. Genetics 176: 2027–2033.

Smolikov, S., A. Eizinger, K. Schild-Prufert, A. Hurlburt, K. McDonald *et al.*, 2007b SYP-3 restricts synaptonemal complex assembly to bridge paired chromosome axes during meiosis in *Caenorhabditis elegans*. Genetics 176: 2015–2025.

Suwaki, N., K. Klare, and M. Tarsounas, 2011 RAD51 paralogs: roles in DNA damage signalling, recombinational repair and tumorigenesis. Semin. Cell Dev. Biol. 22: 898–905.

Tao, Y., X. Li, Y. Liu, J. Ruan, S. Qi *et al.*, 2012 Structural analysis of Shu proteins reveals a DNA binding role essential for resisting damage. J. Biol. Chem. 287: 20231–20239.

Taylor, M. R., M. Spirek, K. R. Chaurasiya, J. D. Ward, R. Carzaniga *et al.*, 2015 Rad51 paralogs remodel pre-synaptic Rad51 filaments to stimulate homologous recombination. Cell 162: 271–286.

Thacker, J., 2005 The RAD51 gene family, genetic instability and cancer. Cancer Lett. 219: 125–135.

Vaz, F., H. Hanenberg, B. Schuster, K. Barker, C. Wiek *et al.*, 2010 Mutation of the RAD51C gene in a Fanconi anemia-like disorder. Nat. Genet. 42: 406–409.

Wagner, C. R., L. Kuervers, D. L. Baillie, and J. L. Yanowitz, 2010 xnd-1 regulates the global recombination landscape in Caenorhabditis elegans. Nature 467: 839–843.

Wang, A. T., T. Kim, J. E. Wagner, B. A. Conti, F. P. Lach *et al.*, 2015 A dominant mutation in human RAD51 reveals its function in DNA interstrand crosslink repair independent of homologous recombination. Mol. Cell 59: 478–490.

Ward, J. D., L. J. Barber, M. I. Petalcorin, J. Yanowitz, and S. J. Boulton, 2007 Replication blocking lesions present a unique substrate for homologous recombination. EMBO J. 26: 3384–3396.

Ward, J. D., D. M. Muzzini, M. I. Petalcorin, E. Martinez-Perez, J. S. Martin *et al.*, 2010 Overlapping mechanisms promote postsynaptic RAD-51 filament disassembly during meiotic double-strand break repair. Mol. Cell 37: 259–272.

Yanowitz, J. L., 2008 Genome integrity is regulated by the *Caenorhabditis elegans* Rad51D homolog rfs-1. Genetics 179: 249–262.

Youds, J. L., N. J. O'Neil, and A. M. Rose, 2006 Homologous recombination is required for genome stability in the absence of DOG-1 in *Caenorhabditis elegans*. Genetics 173: 697–708.

Communicating editor: S. K. Sharan

GENETICS

Supporting Information
www.genetics.org/lookup/suppl/doi:10.1534/genetics.115.185827/-/DC1

Promotion of Homologous Recombination by SWS-1 in Complex with RAD-51 Paralogs in *Caenorhabditis elegans*

T. Brooke McClendon, Meghan R. Sullivan, Kara A. Bernstein, and Judith L. Yanowitz

DOI: 10.1534/genetics.115.185827

Supplemental Figure 1

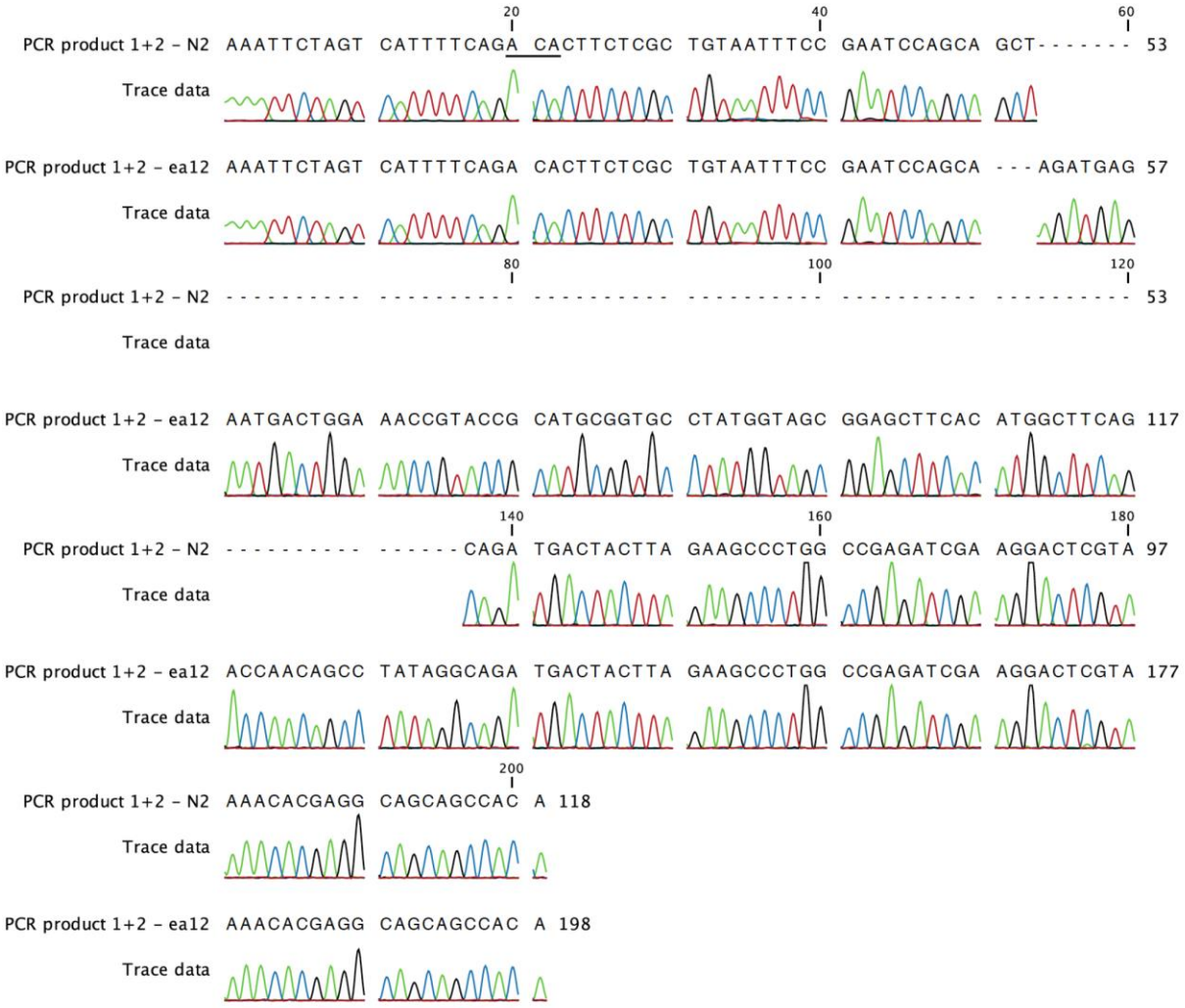

Figure S1. Alignment of *sws-1* exon 2 in N2 and *ea12* mutants.

Sequencing data for exon 2 of *sws-1* in N2 and *sws-1(ea12)* worms. PCR products were amplified with primers 1 and 2 and purified as described in Methods. Line marks both beginning of exon 2 and establishes translation frame.

Supplemental Figure 2

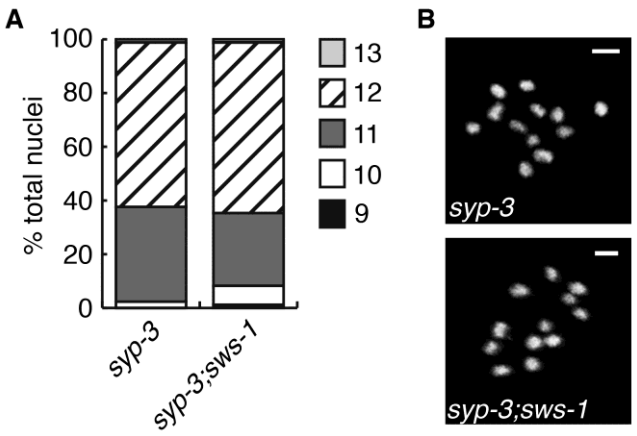

Figure S2. *sws-1* is competent for intersister HR.

A. Quantification of the number of DAPI-staining bodies at diakinesis in *syp-3* and *syp-3;sws-1* germ lines. The -1 and -2 oocytes were used for analysis (n=85 nuclei for both *syp-3* and *syp-3;sws-1*). B. Representative images of -1 oocytes showing 12 condensed univalents. Scale bar is 2 μm.

Supplemental Figure 3

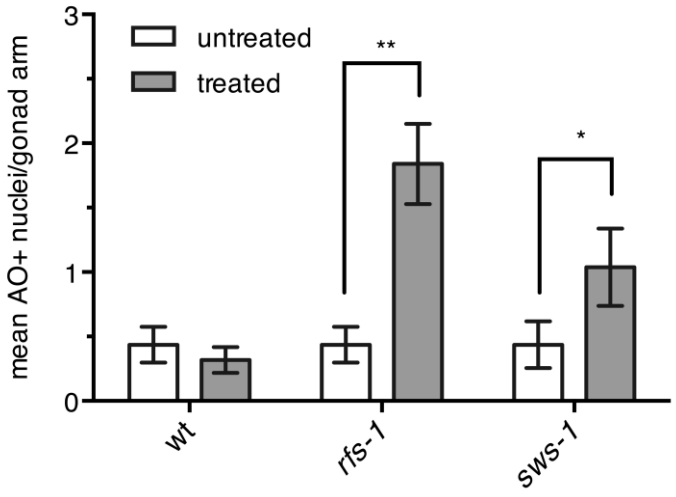

Figure S3. Apoptosis increases in response to CPT in *rfs-1* and *sws-1* germ lines. Apoptosis in wt, *rfs-1*, and *sws-1* germ lines as determined by retention of acridine orange (AO) staining. Young adult hermaphrodites were treated with 0 (untreated) or 500 nM (treated) CPT and stained with AO in the timeframe corresponding to assessment of progeny survival (Figure 5) as described in Materials and Methods. The data are presented as mean AO-positive nuclei per gonad arm ± SEM for 25 hermaphrodites. * $p<0.05$, ** $p<0.001$, Mann-Whitney.

Figure S4

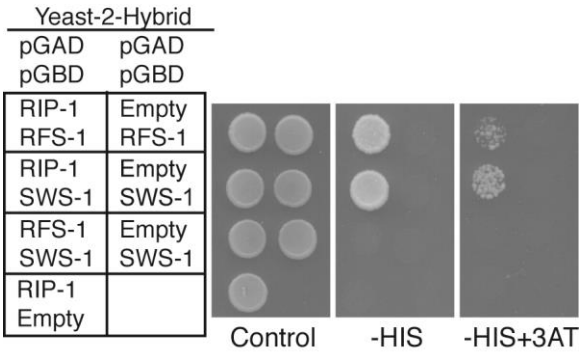

Supplemental Figure 4. SWS-1, RIP-1, RFS-1 Y2H interactions are also observed when the genes are cloned into the opposite pGAD or pGBD vectors shown in Figure 5.

SWS-1 interacts with RIP-1 when RIP-1 is expressed in the pGAD plasmid and SWS-1 is expressed in the pGBD plasmid. SWS-1 does not interact with RFS-1 when RFS-1 is expressed in the pGAD plasmid and SWS-1 is expressed in the pGBD plasmid.

Figure S5

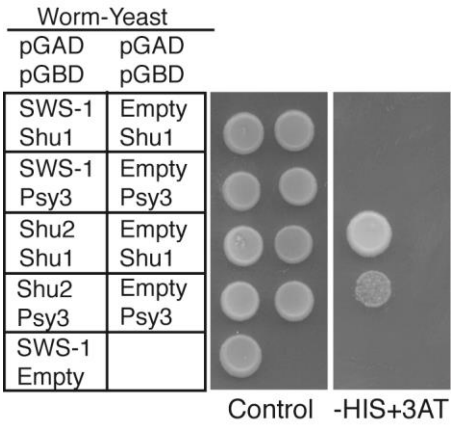

Figure S5. Y2H of SWS-1 with yeast Shu complex components

Interactions between worm SWS-1 and yeast Shu1 or Psy3 were not detected. Controls show known interactions between the yeast SWS1 family member, Shu2, and its binding partners Shu1 and Psy3 on -HIS+3AT.

Table S1. Strains generated for this study

STRAIN	GENOTYPE	REFERENCE IN TEXT
QP1203	*helq-1(tm2134)* III;*sws-1(ea12)* V	*helq-1;sws-1*
QP1204	*rfs-1(ok1372)* III;*sws-1(ea12)* V	*rfs-1;sws-1*
QP1205	*rip-1(tm2948)* III;*sws-1(ea12)* V	*rip-1;sws-1*
QP1206	*rfs-1(ok1372),rip-1(tm2948)* III;*sws-1(ea12)* V	*rfs-1,rip-1;sws-1*
QP1208	*sws-1(ea12)* V	*sws-1*
QP1179	*sws-1(ea12)* V;*unc-58(e665)* X	*sws-1;unc-58*
QP1234	*dog-1(gk10)* I;*sws-1(ea12)* V	*dog-1;sws-1*
QP1263	*syp-3(ok758)* I;*sws-1(ea12)* V	*syp-3;sws-1*

Table S2. Primers used in this study

PRIMER	SEQUENCE (5'→3')
sws-1 5' gRNA	AAGTAGTCATCTGAGCTGCGTTTTAGAGCTAGAAATAGCAAGT
sws-1 3' gRNA	AGTGTAAATCCGAAATAGTGTTTTAGAGCTAGAAATAGCAAGT
1	AGCGGGAATTTGAAGATG
2	AGCTGGAAACTCTGAAAC
3	CCCATATTTCCAGTCAACC
4	GTGCCTGGAGTTGGAAAA
SWS-1.C133S.F	CATTATTGTACATCTCCATACTTTCAATC
SWS-1.C133S.R	GATTGAAAGTATGGAGATGTACAATAATG
SWS-1.A156T.F	GTGTTCATATTTTAACTTACTATTTTGC
SWS-1.A156T.R	GCAAAATAGTAAGTTAAAATATGAACAC
RIP-1.F	GCGGGATCCATGTCAGAATCGTGCAATTC
RIP-1.R	GCGGTCGACGAAAATTCATTTAATAAAAACC
RIP-1.D131A.F	GGTCGTCGTGATTGCTTTGAGAGATGAT
RIP-1.D131A.R	ATCATCTCTCAAAGCAATCACGACGACC
RFS-1.F	GCGAATTCATGGATCCTTCTGAGAATGTATTC
RFS-1.R	GAAGATCTTCATTCCACTGCTTTGAGTC

Table S3. One-way ANOVA multiple comparisons of lethality among genetic combinations of *sws-1*, *rfs-1*, and *rip-1*

COMPARISON	MEAN DIFF.	95% CI OF DIFF.	p<0.05
sws-1 vs. *rip-1;sws-1*	5.867	-1.328 to 13.06	No
sws-1 vs. *rip-1*	2.121	-8.095 to 12.34	No
sws-1 vs. *rfs-1,rip-1*	-0.02070	-8.152 to 8.111	No
sws-1 vs. *rfs-1,rip-1;sws-1*	-3.880	-10.45 to 2.689	No
sws-1 vs. *rfs-1*	-0.9106	-9.319 to 7.498	No
sws-1 vs. *rfs-1;sws-1*	0.6105	-7.074 to 8.295	No
rip-1;sws-1 vs. *rip-1*	3.746	-7.013 to 14.50	No
rip-1;sws-1 vs. *rfs-1,rip-1*	-5.888	-14.69 to 2.915	No
rip-1;sws-1 vs. *rfs-1,rip-1;sws-1*	-9.748	-17.13 to -2.363	Yes**
rip-1;sws-1 vs. *rfs-1*	-6.778	-15.84 to 2.282	No
rip-1;sws-1 vs. *rfs-1;sws-1*	-5.257	-13.65 to 3.135	No
rip-1 vs. *rfs-1,rip-1*	-2.142	-13.55 to 9.264	No
rip-1 vs. *rfs-1,rip-1;sws-1*	-6.002	-16.35 to 4.349	No
rip-1 vs. *rfs-1*	-3.032	-14.64 to 8.574	No
rip-1 vs. *rfs-1;sws-1*	-1.511	-12.60 to 9.581	No
rfs-1,rip-1 vs. *rfs-1,rip-1;sws-1*	-3.860	-12.16 to 4.439	No
rfs-1,rip-1 vs. *rfs-1*	0.8899	-8.930 to 10.71	No
rfs-1,rip-1 vs. *rfs-1;sws-1*	-0.6312	-9.838 to 8.576	No
rfs-1,rip-1;sws-1 vs. *rfs-1*	-2.970	-11.54 to 5.601	No
rfs-1,rip-1;sws-1 vs. *rfs-1;sws-1*	-4.491	-12.35 to 3.371	No
rfs-1 vs. *rfs-1;sws-1*	1.521	-7.932 to 10.97	No

Tukey's test performed simultaneously with one-way ANOVA. Asterisks indicate multiplicity adjusted p values (** p<0.01).

Table S4. One-way ANOVA multiple comparisons of male frequency among genetic combinations of *sws-1*, *rip-1*, and *rfs-1*

COMPARISON	MEAN DIFF.	95% CI OF DIFF.	p<0.05
sws-1 vs. *rip-1;sws-1*	-0.2374	-1.177 to 0.7025	No
sws-1 vs. *rip-1*	-1.151	-2.486 to 0.1833	No
sws-1 vs. *rfs-1,rip-1*	-1.568	-2.630 to -0.5058	Yes***
sws-1 vs. *rfs-1,rip-1;sws-1*	-1.798	-2.656 to -0.9398	Yes****
sws-1 vs. *rfs-1*	-1.583	-2.681 to -0.4846	Yes***
sws-1 vs. *rfs-1;sws-1*	-1.152	-2.156 to -0.1480	Yes*
rip-1;sws-1 vs. *rip-1*	-0.914	-2.319 to 0.4914	No
rip-1;sws-1 vs. *rfs-1,rip-1*	-1.331	-2.480 to -0.1808	Yes*
rip-1;sws-1 vs. *rfs-1,rip-1;sws-1*	-1.561	-2.525 to -0.5961	Yes****
rip-1;sws-1 vs. *rfs-1*	-1.346	-2.529 to -0.1622	Yes*
rip-1;sws-1 vs. *rfs-1;sws-1*	-0.9145	-2.011 to 0.1817	No
rip-1 vs. *rfs-1,rip-1*	-0.4167	-1.907 to 1.073	No
rip-1 vs. *rfs-1,rip-1;sws-1*	-0.6467	-1.999 to 0.7054	No
rip-1 vs. *rfs-1*	-0.4317	-1.948 to 1.084	No
rip-1 vs. *rfs-1;sws-1*	-0.0005128	-1.449 to 1.448	No
rfs-1,rip-1 vs. *rfs-1,rip-1;sws-1*	-0.23	-1.314 to 0.8541	No
rfs-1,rip-1 vs. *rfs-1*	-0.015	-1.298 to 1.268	No
rfs-1,rip-1 vs. *rfs-1;sws-1*	0.4162	-0.7865 to 1.619	No
rfs-1,rip-1;sws-1 vs. *rfs-1*	0.215	-0.9046 to 1.335	No
rfs-1,rip-1;sws-1 vs. *rfs-1;sws-1*	0.6462	-0.3808 to 1.673	No
rfs-1 vs. *rfs-1;sws-1*	0.4312	-0.8037 to 1.666	No

Tukey's test performed simultaneously with one-way ANOVA. Asterisks indicate multiplicity adjusted p values (* p<0.05, ** p<0.01, *** p<0.001, ****p<0.0001).